Zeitschrift: Schweizerische mineralogische und petrographische Mitteilungen = Bulletin suisse de minéralogie et pétrographie

Band: 74 (1994)

Heft: 2

Artikel: Crystal chemistry of diopsides from garnet lherzolites (Cima Lunga/Adula Nappe, Central Alps)

Autor: Nimis, Paolo

DOI: https://doi.org/10.5169/seals-56340

SCHWEIZ. MINERAL. PETROGR. MITT. 74, 181–190, 1994

Crystal chemistry of diopsides from garnet lherzolites (Cima Lunga/Adula Nappe, Central Alps)

by *Paolo Nimis*[1]

Abstract

The first crystal chemical data on garnet peridotite clinopyroxene are presented through the study of a suite of diopsides from metamorphic garnet lherzolites from the Cima Lunga/Adula Nappe, Central Alps (CL-Cpx).

CL-Cpx have low Al^{IV} occupancies and moderate, though variable, Na and Al^{VI} contents. Small Al^{IV} may be due to fractionation of Al_2O_3 into coexisting garnet ± amphibole, and involves low T site volumes (2.218–2.226 Å^3). Contraction of the almost Si-saturated tetrahedron favours expansion of adjacent M1 polyhedron and requires relatively low Al^{VI}. This produces relatively large cell volumes (435.6–438.3 Å^3), despite the relatively high-pressure origin (garnet stability field).

The crystal chemical evolution of CL-Cpx is characterized by a rimward $NaAl^{VI}$ depletion causing significant cell volume increase. Fe^{3+} appears not to be negligible in CL-Cpx and decreases as volumes increase. These changes are consistent with a decompressional evolution involving breakdown of garnet and formation of a spinel + amphibole-bearing assemblage. The different $NaAl^{VI}$ contents of the clinopyroxenes from the different localities may reflect either different original equilibration pressures or compositional effects, such as different H_2O contents.

Petrographic features and mineral chemistry suggest that breakdown of garnet occurred at $T < 800$ °C (perhaps even lower than 700 °C) and $P < 16$ kbar.

Keywords: clinopyroxene, crystal chemistry, garnet peridotites, Cima Lunga/Adula nappe, Central Alps.

Introduction

Abundant crystal structural data available on C2/c clinopyroxene (Cpx; Fig. 1) (Carbonin et al., 1991, and references therein) show that cation substitution mechanisms depend on either the physico-chemical conditions of formation or the intracrystalline constraints induced by geometrical variations of the coordination polyhedra. Detailed crystal chemical studies are therefore essential to understand the behaviour of Cpx in different petrogenetic environments.

Available data on peridotite Cpx are related to spinel- or garnet + spinel-bearing nodules (Dal Negro et al., 1984; Cundari et al., 1986; Principalle et al., 1989; Nimis, 1994), representing mantle melting residua, and to massif lherzolites reequilibrated in the plagioclase facies (Nimis, 1994). In the present work the first crystal chemical data on garnet peridotite Cpx are presented through the study of a suite of diopsides from metamorphic garnet lherzolites from the Cima Lunga/Adula Nappe (Central Alps), hereafter labelled CL-Cpx. Moreover, the structural refinement provides an independent evaluation of the chemical composition (Dal Negro et al., 1982) and may therefore be used to constrain site occupancies and chemical data, which are crucial to geothermometric estimates. A list of abbreviations used in the text is given in table 1.

Geological and petrological outline

Four garnet peridotites from Cima di Gagnone (CG), Verzasca Valley, Alpe Arami (AA), northwest of Bellinzona, Switzerland, and M. Duria (MD), north of Lago di Como, Italy, were selected for crystal chemical analysis. These localities belong to the same tectonic unit, namely the Cima Lunga/Adula nappe.

Detailed geological and petrological outlines

[1] Dipartimento di Mineralogia e Petrologia, Università di Padova, Corso Garibaldi 37, I-35122 Padova, Italy.

Tab. 1 Legend to abbreviations.

Cpx	clinopyroxene(s);
CL	Cima Lunga/Adula;
AA	Alpe Arami;
MD	M. Duria;
CG	Cima di Gagnone;
T	temperature;
P	pressure;
a.f.u.	atoms per formula unit;
calc.	calculated;
obs.	observed;
tot.	total;
e^-_s	mean electron density on s site;
Vc, VM1, VT, VM2	cell and site volumes;
<M1-O>	mean M1 cation-oxygen bond length;
$<T\text{-}O_{nbrg}>$	mean T cation-*non bridging* oxygen (O1 and O2) bond length;
R^{3+}	sum of $(Al^{3+} + Fe^{3+} + Cr^{3+} + Ti^{4+})$ in M1 site;
$Al^{IV,VI}$	Al in tetrahedral (T site) or octahedral (M1 site) coordination.

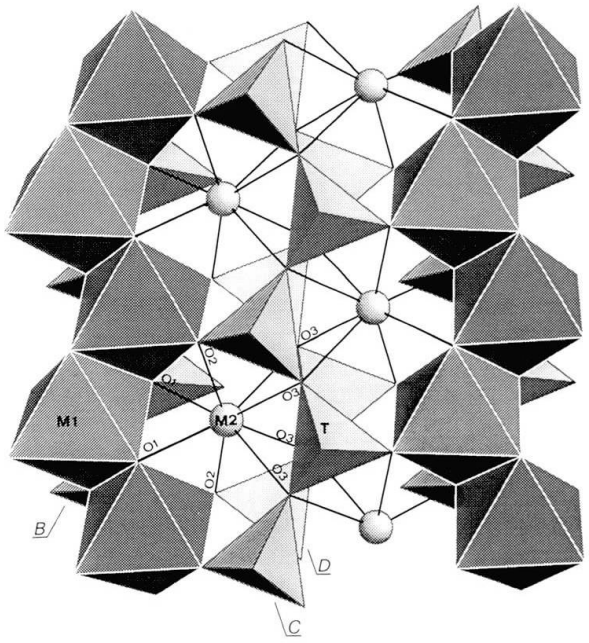

Fig. 1 Perspective view of C2/c pyroxene structure perpendicular to the (100) plane with atom and silicate chain nomenclature (Burnham et al., 1967) adopted in this paper.

were given e.g. by Evans and Trommsdorff (1978), Fumasoli (1974), Ernst (1978), and Trommsdorff (1990). Briefly, the garnet peridotites outcrop as small lenses or macroboudins accompanied by a variety of rocks comprising leucocratic migmatitic gneisses, semi-pelitic gneisses, marbles and mafic dykes (eclogites and metarodingites). At AA and MD garnet develops as subhedral porphyroblasts. At CG elongate poikiloblastic garnet is confined to strongly deformed bands (Piccardo et al., 1993) and overgrows preexisting folds marked by an amphibole + pyroxenes ± olivine-bearing assemblage.

The garnet peridotites are related to a regional eclogitic-facies metamorphism (Heinrich, 1986). $P > 20$ kbar and $T \approx 800$ °C, consistent with the *P-T* derived for the associated eclogites, were estimated by Evans and Trommsdorff (1978). More severe conditions were inferred for AA by Carswell and Gibb (1980; 836–893 °C, 29.4–33.0 kbar) and by Ernst (1981; 950 °C, 40 kbar). During the subsequent meso-Alpine amphibolite-facies metamorphism, garnet breaks down into a spinel + amphibole kelyphite and, in H_2O-rich domains, into late chlorite clots. Kelyphite around garnet is generally less developed at CG than at AA and MD, but is present in all the investigated specimens.

The close association of rocks pertaining to different lithospheric levels has been interpreted as a *lithospheric mélange* formed in a subduction zone through tectonic erosion (Trommsdorff, 1990), followed by tectonic exhumation and very rapid uplift (Vance and O'Nions, 1992). Evidence of Eocene/Oligocene age for the subduction-related eclogitic metamorphism has been recently provided by Gebauer et al. (1992) and by Becker (1993). The possibility that AA garnet peridotites may have much older protoliths and may have experienced other high-pressure events before Eocene (at 1.2 Ga and 650 Ma) has been proposed by Gebauer et al. (1992) and by Trommsdorff (1990).

Analytical methods

Fragments (0.1–0.2 mm) of Cpx grains were hand-picked from ca. 150 mm-thick rock sections, choosing optically homogeneous core and rim portions. Structural data (Tab. 2) were obtained through single-crystal X-ray diffraction on a Siemens AED II four-circle automated diffractometer with MoKα radiation monochromatized with a flat graphite crystal following procedures described by Dal Negro et al. (1982). EDS electron microprobe analyses of the same crystals used for structural refinement were carried out with an ETEC-AUTOSCAN system operating at 15 kV and 5 nA, equipped with an ORTEC EEDS spectrometer. A MAGIC program (Colby, 1972) in the ORTEC MAGIC IVM version was used to

Tab. 2 Structural refinement data and geometrical parameters of Cima Lunga clinopyroxenes. Bond lengths and cell parameters in Å, site and cell volumes in Å^3; estimated standard deviations (in parentheses) refer to the last digit. Atom nomenclature after BURNHAM et al. (1967).

	9-5-2A Alpe Arami						9-88 Alpe Arami			
	1		2		3		1		2	
	core	rim	core	rim	core	rim	core	rim	core	rim
a	9.712(1)	9.717(2)	9.718(1)	9.713(1)	9.715(2)	9.721(2)	9.731(1)	9.737(1)	9.734(2)	9.736(2)
b	8.882(2)	8.893(3)	8.888(1)	8.888(1)	8.891(3)	8.892(2)	8.901(2)	8.908(1)	8.906(2)	8.906(2)
c	5.257(1)	5.261(1)	5.262(1)	5.265(0)	5.259(1)	5.257(1)	5.259(1)	5.257(0)	5.260(1)	5.263(1)
β(°)	106.15(1)	106.14(1)	106.17(1)	106.19(1)	106.16(2)	106.15(1)	106.06(1)	106.02(1)	106.04(1)	106.04(1)
Vc	435.62	436.68	436.49	435.71	436.31	436.47	437.76	438.28	438.25	438.54
obs. refl. *	547	529	574	556	515	484	560	587	540	577
R(%)	2.1	2.5	2.1	1.9	2.9	3.1	2.0	1.7	2.2	2.5
M1-O2	2.030(2)	2.038(2)	2.032(2)	2.031(1)	2.034(2)	2.034(2)	2.041(2)	2.045(1)	2.043(2)	2.045(2)
M1-O1A2	2.047(2)	2.051(2)	2.046(1)	2.045(1)	2.042(2)	2.045(3)	2.053(2)	2.057(1)	2.054(2)	2.057(2)
M1-O1A1	2.109(1)	2.111(2)	2.111(1)	2.114(1)	2.114(2)	2.121(3)	2.121(1)	2.120(1)	2.114(2)	2.120(2)
<M1-O>	2.062(4)	2.067(4)	2.063(4)	2.063(3)	2.063(5)	2.067(6)	2.072(4)	2.074(2)	2.070(4)	2.074(4)
VM1	11.59(1)	11.67(1)	11.61(1)	11.62(0)	11.61(1)	11.67(1)	11.76(1)	11.80(0)	11.74(1)	11.80(1)
M2-O2	2.347(2)	2.349(2)	2.347(1)	2.341(2)	2.346(3)	2.339(3)	2.340(2)	2.341(1)	2.337(2)	2.342(2)
M2-O1	2.368(2)	2.367(2)	2.364(1)	2.363(2)	2.364(2)	2.360(3)	2.361(2)	2.361(1)	2.363(2)	2.361(2)
M2-O3C1	2.547(2)	2.549(2)	2.550(2)	2.548(1)	2.551(2)	2.554(3)	2.559(2)	2.563(1)	2.562(2)	2.561(2)
M2-O3C2	2.728(2)	2.731(2)	2.732(1)	2.733(1)	2.734(2)	2.730(2)	2.729(1)	2.728(1)	2.728(2)	2.731(2)
VM2	25.72(1)	25.77(1)	25.73(1)	25.67(1)	25.75(1)	25.66(2)	25.72(1)	25.74(1)	25.71(1)	25.77(1)
T-O2	1.587(2)	1.586(2)	1.589(2)	1.588(2)	1.584(3)	1.585(3)	1.589(2)	1.588(1)	1.590(2)	1.586(2)
T-O1	1.606(1)	1.605(1)	1.609(1)	1.605(1)	1.610(1)	1.607(2)	1.603(1)	1.603(1)	1.608(2)	1.605(2)
T-O3A1	1.662(2)	1.663(2)	1.665(1)	1.661(1)	1.660(2)	1.663(2)	1.664(1)	1.667(1)	1.667(2)	1.667(2)
T-O3A2	1.679(2)	1.683(3)	1.680(2)	1.681(2)	1.684(4)	1.680(4)	1.685(2)	1.683(1)	1.683(2)	1.683(2)
<T-O_{nbrg}>	1.597	1.595	1.599	1.597	1.597	1.596	1.596	1.595	1.599	1.596
<T-O_{brg}>	1.670	1.673	1.672	1.671	1.672	1.671	1.675	1.675	1.675	1.675
VT	2.219(2)	2.221(3)	2.227(2)	2.220(2)	2.223(3)	2.219(4)	2.225(2)	2.224(1)	2.231(2)	2.226(2)
tilt(°)	2.51	2.37	2.44	2.51	2.39	2.66	2.54	2.59	2.61	2.57
kink(°)	166.9	166.9	167.0	166.9	166.8	166.6	166.4	166.4	166.3	166.5

* : $I_{hkl} > 3\sigma(I_{hkl})$

Tab. 2 (cont.)

	264.3 Duria				160-4-8 Gagnone			
	1		2		1		2	
	core	rim	core	rim	core	rim	core	rim
a	9.732(1)	9.737(1)	9.725(1)	9.729(1)	9.732(1)	9.736(1)	9.731(1)	9.736(2)
b	8.903(2)	8.914(2)	8.902(2)	8.905(2)	8.809(1)	8.913(2)	8.908(1)	8.908(2)
c	5.255(2)	5.256(1)	5.257(1)	5.258(1)	5.254(1)	5.257(1)	5.255(0)	5.259(1)
β(°)	106.06(1)	105.99(1)	106.06(1)	106.06(1)	106.04(1)	105.98(1)	106.05(1)	106.02(1)
Vc	437.53	438.52	437.30	437.75	437.80	438.55	437.75	438.41
obs. refl. *	511	507	540	547	578	553	569	596
R(%)	2.4	3.3	2.3	2.4	2.0	2.4	1.8	2.0
M1-O2	2.043(2)	2.044(2)	2.038(2)	2.041(2)	2.046(2)	2.045(2)	2.044(1)	2.045(2)
M1-O1A2	2.052(2)	2.059(3)	2.053(2)	2.056(2)	2.054(2)	2.059(2)	2.056(1)	2.056(2)
M1-O1A1	2.121(2)	2.123(3)	2.116(2)	2.115(2)	2.120(1)	2.122(2)	2.119(1)	2.120(1)
<M1-O>	2.072(4)	2.075(6)	2.069(4)	2.071(4)	2.073(4)	2.075(4)	2.073(2)	2.074(4)
VM1	11.77(1)	11.83(1)	11.71(1)	11.75(1)	11.79(1)	11.82(1)	11.78(0)	11.79(1)
M2-O2	2.336(2)	2.338(3)	2.341(2)	2.339(2)	2.336(2)	2.339(2)	2.337(1)	2.339(2)
M2-O1	2.363(2)	2.360(3)	2.360(2)	2.363(2)	2.361(2)	2.360(2)	2.361(1)	2.363(2)
M2-O3C1	2.559(2)	2.561(3)	2.557(2)	2.561(2)	2.562(2)	2.565(2)	2.561(1)	2.561(2)
M2-O3C2	2.729(2)	2.729(2)	2.729(2)	2.730(2)	2.729(2)	2.728(2)	2.729(1)	2.729(1)
VM2	25.70(1)	25.70(2)	25.67(1)	25.74(1)	25.70(1)	25.73(1)	25.70(1)	25.73(1)
T-O2	1.586(2)	1.589(3)	1.588(2)	1.589(2)	1.586(2)	1.587(2)	1.586(1)	1.588(1)
T-O1	1.601(1)	1.601(2)	1.606(2)	1.604(2)	1.602(1)	1.600(2)	1.604(1)	1.603(1)
T-O3A1	1.664(2)	1.667(2)	2.665(2)	1.663(2)	1.664(2)	1.666(2)	1.664(1)	1.666(1)
T-O3A2	1.683(3)	1.682(4)	2.683(2)	1.684(2)	1.684(2)	1.686(2)	1.684(1)	1.685(2)
$<T\text{-}O_{nbrg}>$	1.594	1.595	1.597	1.596	1.594	1.593	1.595	1.596
$<T\text{-}O_{brg}>$	1.674	1.674	1.674	1.674	1.674	1.676	1.674	1.676
VT	2.218(3)	2.223(4)	2.226(2)	2.224(2)	2.220(2)	2.223(2)	2.222(1)	2.226(2)
tilt(°)	2.64	2.66	2.54	2.61	2.52	2.64	2.52	2.54
kink(°)	166.5	166.6	166.6	166.3	166.3	166.2	166.3	166.4

* : $I_{hkl} > 3\sigma(I_{hkl})$

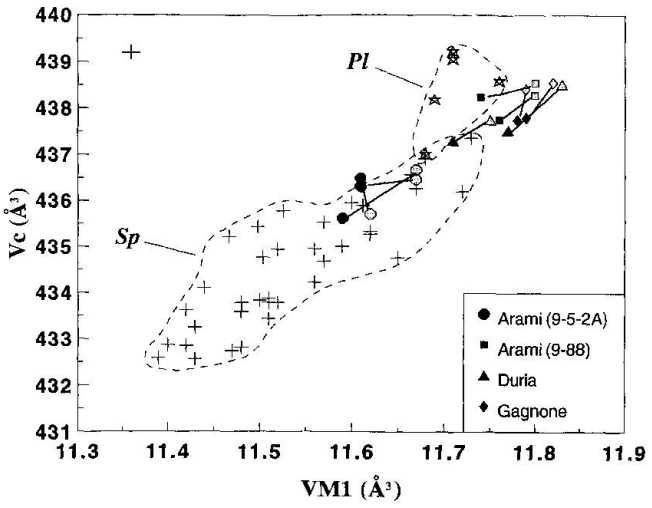

Fig. 2 Cell volume vs M1 volume relationship in peridotite clinopyroxenes. *Sp:* spinel peridotite field (crosses) after DAL NEGRO et al. (1984), CUNDARI et al. (1986), and PRINCIVALLE et al. (1989). *Pl:* plagioclase peridotite field *(stars)* after NIMIS (1994). *Solid lines:* core-rim trends for Cima Lunga samples (cores: filled symbols; rims: open symbols). Error bars correspond to 2 σ.

convert elemental X-ray counts into weight % oxides. Results are considered accurate to within 2–5 relative % for major elements and ca. 9% for minor elements. Neither inclusions nor significant zoning were detected in the examined crystal fragments. The program of PAPIKE et al. (1974) was used to convert weight % oxides into atoms per formula unit and to make a first estimation of Fe^{3+} with the charge-balance method. Site partitionings were calculated according to DAL NEGRO et al. (1982). These authors showed that site partitioning can be constrained on the basis of <M1–O> mean distance and mean electron densities on M2 and M1 sites, both derived from structural refinement, through the equations:

(1) $18\ Ca + 10\ Na + 23\ Mn + 24\ Fe^{2+}_{M2} + 10\ Mg_{M2} = e^{-}_{M2}$;

(2) $10\ Mg_{M1} + 24\ Fe^{2+}_{M1} + 23\ Fe^{3+} + 10\ Al^{VI} + 21\ Cr + 18\ Ti = e^{-}_{M1}$;

(3) $2.081\ Mg_{M1} + 2.126\ Fe^{2+}_{M1} + 2.03\ Fe^{3+} + 1.93\ Al^{VI} + 2.01\ Cr + 1.99\ Ti = <M1\text{-}O>$.

Cation fractions are multiplied by their respective electrons in the former two equations, and by their octahedral cation-oxygen mean distance in the latter. This is particularly important for Fe^{3+} estimation, as Fe–O bond lengths are different depending on iron oxidation state (Fe^{2+}–O = 2.126 Å; Fe^{3+}–O = 2.030 Å; DAL NEGRO et al., 1982). This does not mean that the structural refinement provides a direct measure of Fe^{2+}/Fe^{3+} partitioning. Nevertheless, good-quality chemical analyses should fit the above equations within analytical uncertainties. Structural data will be tentatively used to constrain Fe^{3+} estimates in both Cpx cores and rims by selecting those partitionings that yield the best match between observed and calculated values of <M1-O> and electron densities ($<M1\text{-}O>_{calc} - <M1\text{-}O>_{obs} < 0.003$ Å; $(e^{-}_{calc.} - e^{-}_{obs.})_{M1+M2} < 0.3\ e^{-}$; Tab. 3). These partitionings will be referred to as "constrained analyses".

Crystal chemistry

Studies on Cpx from peridotites equilibrated in the spinel (DAL NEGRO et al., 1984; CUNDARI et al., 1986; PRINCIVALLE et al., 1989), plagioclase and garnet + spinel facies (NIMIS, 1994) showed that, in general, Cpx adapts itself to increasing pressure by reducing site and cell volumes. The largest variations involve the M1 site, whose volume is linearly correlated with the cell volume (Fig. 2). Substitution $(Na\ Ca_{-1})_{M2}\ (Al^{VI}\ Mg_{-1})_{M1}$ is the main responsible for these volume reductions and is therefore strongly pressure-dependent.

CL-Cpx conform to the linear cell volume vs M1 volume relationship (Fig. 2). The M1 volume is correlated with the content of small-sized and high-charged R^{3+}_{M1} (= $Al^{VI} + Fe^{3+} + Cr^{3+} + Ti^{4+}$), mainly Al^{VI} (Fig. 3). Substitution of Na^{+} for Ca^{2+} in M2 site balances the charge excess determined by substitution of R^{3+} for bivalent cations in M1 (Tab. 3). Geometrical variations of M2 and T polyhedra are small (Tab. 2), M2 being little affected by the main $(Na\ Ca_{-1})_{M2}$ substitution occurring in the site, and Al^{IV} in the T site being very low and little variable (0.006–0.040 a.f.u.). A common rimward trend towards higher M1 and cell volumes is characteristic to all specimens, but Cpx from specimen 9-5-2A (Arami) are distinct for their smaller cell and M1 volumes (Fig. 2). The other samples show relatively high M1 volumes but have lower cell volumes with respect to plagioclase peridotite Cpx with similar M1, because of very small tetrahedron (VT = 2.218–2.231 Å³). Fe^{3+} appears not to be negligible in the studied Cpx and decreases as volumes increase (Fig. 3). This is more evident if only "constrained analyses" are considered.

Relatively large M1 site of CL-Cpx is related to contraction of the almost Si-saturated T polyhedron (Fig. 4). Shortening of T-O1 and T-O2 ($<T\text{-}O_{nbrg}>$) distances, which are the most sensitive to $(Al^{IV}\ Si_{-1})_T$ substitution, is counterbalanced by lengthening of <M1-O>. A similar relationship, but at lower pressure and for higher Fe^{2+}_{M1} (i.e. longer <M1-O>), occurs in Cpx from volcanic rocks (DAL NEGRO et al., 1989). Note that more

Tab. 3 Microprobe analyses and site partitionings of Cima Lunga clinopyroxenes.

	9-5-2A Alpe Arami						9-88 Alpe Arami			
	1		2		3		1		2	
	core	rim	core	rim	core	rim	core	rim	core	rim
SiO_2	54.33	55.07	54.88	54.86	54.22	55.15	54.74	55.05	54.51	54.75
Al_2O_3	2.76	2.32	2.66	2.31	2.46	2.01	1.88	1.51	1.60	1.65
FeO	2.49	2.15	2.55	2.29	2.48	2.54	2.33	2.22	2.41	2.29
MgO	15.71	16.14	16.07	16.06	15.90	16.39	16.68	17.59	17.28	17.04
MnO	0.08	0.29	0.06	0.09	0.13	0.11	0.08	0.08	0.07	0.06
TiO_2	0.36	0.21	0.14	0.10	0.24	0.09	0.29	0.13	0.12	0.14
Cr_2O_3	1.44	1.70	1.48	1.63	1.55	1.56	1.42	0.90	1.66	1.62
CaO	20.42	20.88	20.68	21.06	20.38	21.21	21.85	22.30	22.06	22.51
Na_2O	2.09	1.85	2.05	1.88	1.98	1.67	1.26	0.86	1.03	0.93
Σ	99.68	100.61	100.57	100.28	99.34	100.73	100.53	100.64	100.74	100.99
T										
Si	1.967	1.978	1.968	1.975	1.970	1.980	1.972	1.978	1.960	1.967
Al^{IV}	0.033	0.022	0.032	0.025	0.030	0.020	0.028	0.022	0.040	0.033
Σ	2.000	2.000	2.000	2.000	2.000	2.000	2.000	2.000	2.000	2.000
M1										
Mg	0.823	0.843	0.829	0.842	0.841	0.862	0.876	0.904	0.886	0.876
Fe^{2+}	0.007	0.012	0.000	0.005	0.000	0.004	0.016	0.016	0.005	0.030
Fe^{3+}	0.034	0.015	0.045	0.031	0.031	0.023	0.008	0.008	0.031	0.008
Al^{VI}	0.085	0.076	0.080	0.073	0.076	0.065	0.052	0.042	0.028	0.036
Ti	0.010	0.006	0.004	0.003	0.007	0.002	0.008	0.004	0.003	0.004
Cr	0.041	0.048	0.042	0.046	0.045	0.044	0.040	0.026	0.047	0.046
Σ	1.000	1.000	1.000	1.000	1.000	1.000	1.000	1.000	1.000	1.000
R^{3+}	0.170	0.145	0.171	0.153	0.159	0.134	0.108	0.080	0.109	0.094
M2										
Ca	0.792	0.804	0.795	0.813	0.793	0.816	0.843	0.858	0.850	0.866
Na	0.147	0.129	0.143	0.131	0.140	0.116	0.088	0.060	0.072	0.065
Fe^{2+}	0.034	0.038	0.031	0.033	0.044	0.050	0.046	0.043	0.037	0.030
Mg	0.025	0.020	0.029	0.020	0.019	0.015	0.021	0.037	0.039	0.038
Mn	0.002	0.009	0.002	0.003	0.004	0.003	0.002	0.002	0.002	0.002
Σ	1.000	1.000	1.000	1.000	1.000	1.000	1.000	1.000	1.000	1.000
Δe^- †	0.03	0.10	0.15	–0.08	–0.02	0.08	–0.01	–0.13	0.13	0.34
Δ<M1-O> ‡	0.001	–0.002	0.000	0.002	0.001	0.000	–0.002	–0.001	0.002	–0.001

†: $e^-_{calc.} - e^-_{obs.\ (M1+M2)}$ after DAL NEGRO et al. (1982);
‡: $<M1\text{-}O>_{calc.} - <M1\text{-}O>_{obs.}$ after DAL NEGRO et al. (1982).

Tab. 3 (cont.)

	264.3 Duria				160-4-8 Gagnone			
	1		2		1		2	
	core	rim	core	rim	core	rim	core	rim
SiO_2	55.12	55.59	55.10	54.11	55.68	55.51	55.20	55.70
Al_2O_3	1.39	0.81	1.17	1.30	1.15	1.01	0.99	0.97
FeO	2.38	2.18	2.66	2.38	2.21	2.08	2.60	2.38
MgO	17.16	17.72	17.16	17.09	17.68	17.70	17.55	17.23
MnO	0.02	0.10	0.44	0.33	0.08	0.23	0.29	0.05
TiO_2	0.03	0.09	0.06	0.10	0.02	0.17	0.08	0.07
Cr_2O_3	1.42	0.92	1.70	1.64	0.53	0.81	0.38	0.62
CaO	21.95	22.91	21.21	22.01	22.68	22.52	22.73	22.83
Na_2O	1.12	0.81	1.30	1.00	0.91	0.84	1.00	1.12
Σ	100.59	101.13	100.80	99.96	100.94	100.87	100.82	100.97
T								
Si	1.983	1.989	1.980	1.963	1.978	1.991	1.979	1.994
Al^{IV}	0.017	0.011	0.020	0.037	0.022	0.009	0.021	0.006
Σ	2.000	2.000	2.000	2.000	2.000	2.000	2.000	2.000
M1								
Mg	0.902	0.927	0.891	0.873	0.910	0.922	0.910	0.900
Fe^{2+}	0.004	0.009	0.000	0.022	0.005	0.015	0.002	0.018
Fe^{3+}	0.011	0.012	0.029	0.037	0.042	0.002	0.055	0.027
Al^{VI}	0.042	0.024	0.030	0.018	0.027	0.033	0.020	0.035
Ti	0.001	0.002	0.002	0.003	0.001	0.005	0.002	0.002
Cr	0.040	0.026	0.048	0.047	0.015	0.023	0.011	0.018
Σ	1.000	1.000	1.000	1.000	1.000	1.000	1.000	1.000
R^{3+}	0.094	0.064	0.109	0.105	0.085	0.063	0.088	0.082
M2								
Ca	0.846	0.878	0.817	0.855	0.886	0.865	0.873	0.876
Na	0.078	0.056	0.091	0.070	0.062	0.058	0.069	0.078
Fe^{2+}	0.057	0.044	0.051	0.032	0.019	0.045	0.020	0.026
Mg	0.018	0.019	0.028	0.033	0.031	0.025	0.029	0.018
Mn	0.001	0.003	0.013	0.010	0.002	0.007	0.009	0.002
Σ	1.000	1.000	1.000	1.000	1.000	1.000	1.000	1.000
Δe^- †	-0.08	0.04	0.07	0.47	0.40	0.01	0.34	0.35
Δ<M1–O> ‡	-0.001	0.000	0.002	0.003	0.001	-0.001	0.001	0.000

†: $e^-_{calc.} - e^-_{obs.\ (M1+M2)}$ after DAL NEGRO et al. (1982);
‡: $<M1–O>_{calc.} - <M1–O>_{obs.}$ after DAL NEGRO et al. (1982).

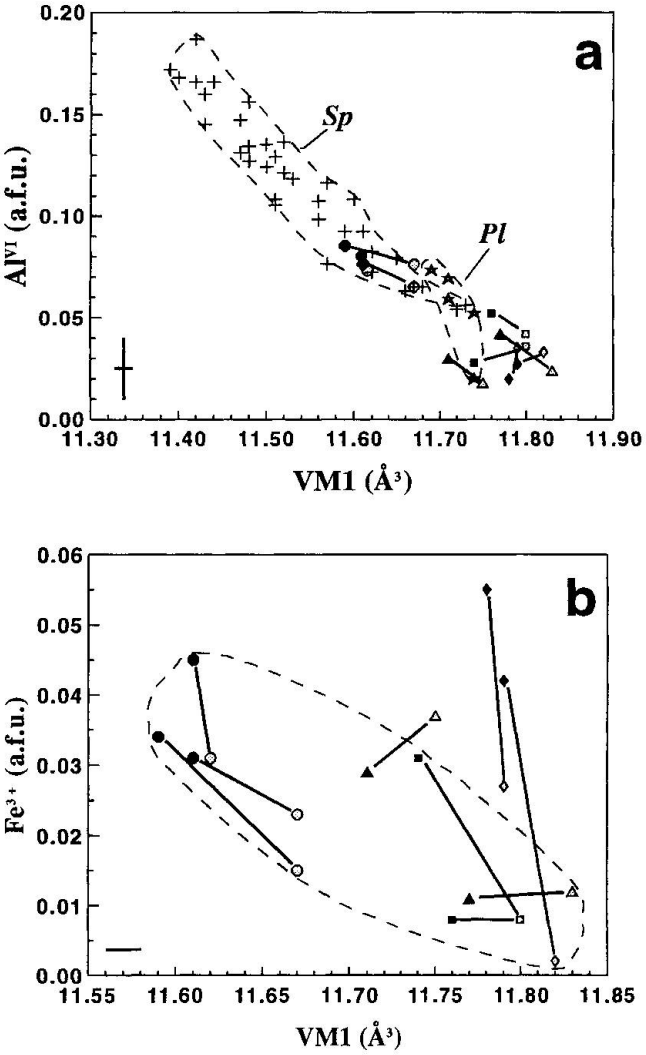

Fig. 3 (a) Al^{VI} vs M1 volume in peridotite clinopyroxenes. Fields as in figure 2. (b) Fe^{3+} vs M1 volume in Cima Lunga clinopyroxenes. *Dashed line* encloses "constrained analyses" (see text). All other symbols as in figure 2. Fe^{3+} values may vary over the entire range of the figure as a result of ± 2 wt% relative inaccuracy of SiO_2 detection.

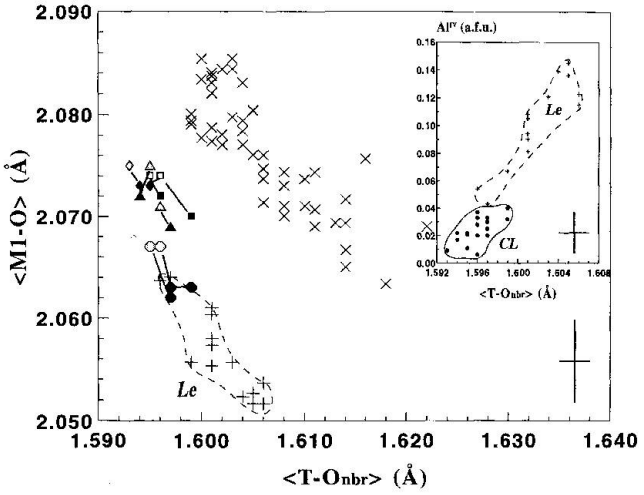

Fig. 4 <M1-O> vs <T-$O_{non\text{-}bridging}$> relationship in peridotite clinopyoxenes. Inset: Al^{IV} vs <T-$O_{non\text{-}bridging}$> (CL: this work). *Le:* Mt. Leura spinel peridotite field *(crosses)* after Dal Negro et al. (1984). *X:* clinopyroxenes from basic volcanics (Dal Negro et al., 1989). Other symbols as in figure 2.

Na-rich suites (e.g. 9-5-2A) show shorter <M1-O> distances (i.e. higher R^{3+}_{M1}) for the same value of <T-O_{nbrg}>.

Evolution of clinopyroxene from Cima Lunga/Adula garnet lherzolites

The main chemical variations of CL-Cpx involve the exchange:

(4) $(Ca\ Na_{-1})_{M2}\,(Mg\ Al_{-1})_{M1}$.

This exchange is responsible for the compositional zoning from cores to rims. In exchange (4), Fe^{3+} may appear instead of Al^{VI}, as its negative correlation with VM1 suggests (Fig. 3). According to Evans and Trommsdorff (1978), exchange (4) may be related to the formation of amphibole. Depletion of Fe^{3+} in Cpx rims may be instead related to the formation of spinel, which is present in the kelyphite replacing garnet as well as in small recrystallized grains near kelyphite. Accordingly, the reequilibrated $NaAl^{VI}$-poor Cpx rims are probably not in equilibrium with the original garnet-peridotite assemblage.

Smaller M1 and cell volumes (i.e. higher $NaAl^{VI}$ contents) of Cpx 9-5-2A (Arami) suggest higher pressure conditions with respect to the other studied samples (Fig. 2). The same holds for Cpx cores with respect to rims in each specimen. It is also worth noting that Cpx from specimens 9-5-2A and 9-88, although both from the same locality, fall in clearly distinct fields (Fig. 2). A possible explanatory hypothesis is that: a) the rimward volume increase in the Cpx from each specimen was related to a pressure decrease, which produced a retrograde metamorphism recorded through the passage from a garnet- to a spinel + amphibole-bearing assemblage and through a rimward decrease of Na and Al^{VI} in Cpx; b) differences in the $NaAl^{VI}$ content of the Cpx from the different localities, and hence their respective positions in the Vc vs VM1 plot (Fig. 2), reflect either different equilibration pressures or compositional effects.

In particular, at CG the presence of a hydrous assemblage prior to garnet formation (Piccardo et al., 1993) might partly explain the low jadeite

content of Cpx cores, as Na and Al would have been fractionated by a coexisting amphibole. A higher original pressure for Arami garnet peridotites would be consistent with the estimates of CARSWELL and GIBB (1980) and ERNST (1981) (see also BECKER, 1993).

Geothermometry

Previous studies suggested $T \geq 800$ °C for Cima Lunga/Adula garnet lherzolites (e.g. EVANS and TROMMSDORFF, 1978; CARSWELL and GIBB, 1980; ERNST, 1981). These estimates were mostly based on pyroxene solvus (Ca-transfer reaction).

As regards garnet-clinopyroxene Fe^{2+}–Mg exchange, KROGH's (1988) geothermometer, which matches best experimental data on garnet lherzolites (BREY and KÖHLER, 1990), yields significantly lower temperatures compared to previous garnet-Cpx geothermometers (< 800 °C; Tab. 4). Moreover, the present work points out that Fe^{3+} is not negligible in CL-Cpx (Tab. 3). Assuming $Fe^{3+}/Fe_{tot.}$ ratio 0.035 in garnet [mean(2) of FETT's (1989) MÖSSBAUER analyses of Arami garnets] and 0.29 in Cpx (mean(13) of "constrained analyses" for CL-Cpx) temperature estimates would be further lowered by some 100 °C (Tab. 4). This is clearly a rough estimate, since $Fe^{3+}/Fe_{tot.}$ ratio may not be the same for the considered specimens (cf. Fig. 3b) and can only be calculated with large uncertainty, as both ferric and ferrous iron are very low in CL-Cpx (Tab. 3). Nevertheless, table 4 gives an idea of the possible bias that may arise from neglecting Fe^{3+}.

The apparently higher closure temperature for Ca transfer (≥ 800 °C) relative to Fe^{2+}–Mg exchange (< 800 °C) would be compatible with a retrograde metamorphic history (SAXENA et al., 1986), consistently with the slower kinetics of the former (e.g. BRADY and MCCALLISTER, 1983; LOOMIS et al., 1985).

Concluding remarks

CL-Cpx are diopsides with low Al^{IV} occupancies and moderate, though variable, Na and Al^{VI} contents. Low Al^{IV} may be due to fractionation of Al_2O_3 into coexisting garnet and (for CG) amphibole, and involves low T volumes. Contraction of the almost Si-saturated tetrahedron favours expansion of adjacent M1 polyhedron and requires relatively low R^{3+}. This may explain the relatively large cell volumes (435.6–438.3 Å^3) of Cpx cores, despite their relatively high-pressure origin (garnet stability field).

Tab. 4 KROGH's (1988) garnet-clinopyroxene thermometry (P = 25 kbar) based on EVANS and TROMMSDORFF's (1978) garnet-pyroxene pairs chemical analyses; (a) all iron as Fe^{2+}; (b) $Fe^{3+}/Fe_{tot.}$ = 0.29 in clinopyroxene and 0.035 in garnet (see text for further explanation).

	Spec.	a	b
Arami	9-5-2C	767	660
Duria	264.3	764	659
Gagnone	160-4-8	717	617

The crystal chemical evolution of CL-Cpx is characterized by a rimward $NaAl^{VI}$ depletion causing sensible cell volume increase. Fe^{3+} appears not to be negligible in CL-Cpx and decreases as volumes increase. These changes are consistent with a decompressional evolution involving breakdown of garnet and formation of a spinel + amphibole-bearing assemblage. The different $NaAl^{VI}$ contents of the Cpx from the different localities, and hence their respective positions in the VM1 vs VC plot (Fig. 2), may reflect either different original equilibration pressures or compositional effects, such as different H_2O contents. Breakdown of garnet may have occurred at $T < 700$ °C. At such a low temperature, $P \approx 16$ kbar would be sufficient to maintain a peridotite within the stability field of garnet (cf. O'NEILL, 1981).

Acknowledgements

I am deeply indebted to V. Trommsdorff for providing the samples and for helpful discussions. I am also grateful to A. Dal Negro and E.M. Piccirillo for their useful suggestions. The financial support of C.N.R. "Centro di Studio per la Geodinamica Alpina" (Padova) and of MURST grants is gratefully acknowledged.

References

BECKER, H. (1993): Garnet peridotite and eclogite Sm–Nd mineral ages from the Lepontine dome (Swiss Alps): new evidence for Eocene high-pressure metamorphism in the central Alps. Geology 21, 599–602.

BRADY, J.B. and MCCALLISTER, R.H. (1983): Diffusion data for clinopyroxene from homogeneization and self-diffusion experiments. Am. Mineral. 68, 95–105.

BREY, G.P. and KÖHLER, T. (1990): Geothermobarometry in four-phase lherzolites II. New thermobarometers, and practical assessment of existing thermobarometers. J. Petrol. 31, 1353–1378.

BURNHAM, C.W., CLARK, J.R., PAPIKE, J.J. and PREWITT, C.T. (1967): A proposed crystallographic nomenclature for clinopyroxene structures. Z. Krist. 125, 109–119.

CARBONIN, S., DAL NEGRO, A., GANEO, S. and PICCIRILLO, E.M. (1991): Influence of magma composition and oxygen fugacity on the crystal structure of C2/c clinopyroxenes from a basalt-pantellerite suite. Contrib. Mineral. Petrol. 108, 34–42.

CARSWELL, D.A. and GIBB, F.G.F. (1980): The equilibration conditions and petrogenesis of European crustal garnet lherzolites. Lithos 13, 19–29.

COLBY, J.W. (1972): A computer program for quantitative electron microprobe analysis. Bell Telephone Laboratories Inc., Allentown, Pennsylvania.

CUNDARI, A., DAL NEGRO, A., PICCIRILLO, E.M., DELLA GIUSTA, A. and SECCO, L. (1986): Intracrystalline relationships in olivine, orthopyroxene, clinopyroxene and spinel from a suite of spinel lherzolite xenoliths from Mt. Noorat, Victoria, Australia. Contrib. Mineral. Petrol. 94, 523–532.

DAL NEGRO, A., CARBONIN, S., MOLIN, G.M., CUNDARI, A. and PICCIRILLO, E.M. (1982): Intracrystalline cation distribution in natural clinopyroxenes of tholeiitic, transitional, and alkaline basaltic rocks. In: Advances in physical geochemistry (SAXENA, S.K., ed.), 2, 117–150, Springer-Verlag, New York.

DAL NEGRO, A., CARBONIN, S., DOMENEGHETTI, C., MOLIN, G.M., CUNDARI, A. and PICCIRILLO, E.M. (1984): Crystal chemistry and evolution of the clinopyroxene in a suite of high pressure ultramafic nodules from the Newer Volcanics of Victoria, Australia. Contrib. Mineral. Petrol. 86, 221–229.

DAL NEGRO, A., MANOLI, S., SECCO, L. and PICCIRILLO, E.M. (1989): Megacrystic clinopyroxenes from Victoria (Australia): crystal chemical comparison of pyroxenes from high and low pressure regimes. Eur. J. Mineral. 1, 105–121.

ERNST, W.G. (1978): Petrochemical study of the lherzolitic rocks from the Western Alps. J. Petrol. 19, 341–392.

ERNST, W.G. (1981): Petrogenesis of eclogites and peridotites from the Western and Ligurian Alps. Am. Mineral. 66, 443–472.

EVANS, B.W. and TROMMSDORFF, V. (1978): Petrogenesis of garnet lherzolite, Cima di Gagnone, Lepontine Alps. Earth Planet. Sc. Lett. 40, 333–348.

FETT, A. (1989): Kristallchemische und petrographische Untersuchungen einiger Lokalitäten des Penninikums im Tessin (Schweiz). Diplomarbeit, Philipps-Universität Marburg.

FUMASOLI, M.W. (1974): Geologie des Gebietes nördlich und südlich der Jorio-Tonale-Linie im Westen von Gravedona (Como, Italia). Dissertation Universität Zürich, 230 pp.

GEBAUER, D., GRÜNENFELDER, M., TILTON, G., TROMMSDORFF, V. and SCHMID, S. (1992): The geodynamic evolution of garnet-peridotites, garnet-pyroxenites and eclogites of Alpe Arami and Cima di Gagnone (Central Alps) from Early Proterozoic to Oligocene. Schweiz. Mineral. Petrogr. Mitt. 72, 107–111.

HEINRICH, C.A. (1986): Eclogite facies regional metamorphism of hydrous mafic rocks in the central Alpine Adula nappe. J. Petrol. 27, 123–154.

KROGH, E.J. (1988): The garnet-clinopyroxene Fe–Mg geothermometer – a reinterpretation of existing experimental data. Contrib. Mineral. Petrol. 99, 44–48.

LOOMIS, T.P., GANGULY, J. and ELPHICK, S.C. (1985): Experimental determination of cation diffusivities in alumino-silicate garnets. Contrib. Mineral. Petrol. 90, 45–51.

NIMIS, P. (1994): Clinopyroxenes from plagioclase peridotites (Zabargad Island, Red Sea) and comparison between high- and low-pressure mantle clinopyroxenes. Mineral. Petrol. (in press).

O'NEILL, H.StC. (1981): The transition between spinel lherzolites and garnet lherzolites, and its use as a geobarometer. Contrib. Mineral. Petrol. 77, 185–194.

PAPIKE, J.J., CAMERON, K. and BALDWIN, K. (1974): Amphiboles and pyroxenes; characterization of other than quadrilateral components and estimates of ferric iron from microprobe data. Geol. Soc. Am. Abstr. with programs 6, 1053–1054.

PICCARDO, G.B., RAMPONE, E., REUSSER, E. and TROMMSDORFF, V. (1993): Garnet peridotites and pyroxenites from the Central Alps: an ion probe investigation on their high pressure minerals. Terra Nova Abst. 4, 20.

PRINCIVALLE, F., SECCO, L. and DEMARCHI, G. (1989): Crystal chemistry of a clinopyroxene series in ultrafemic xenolyths from North-Eastern Brazil. Contrib. Mineral. Petrol. 101, 131–135.

SAXENA, S.K., SYKES, J. and ERIKSSON, G. (1986): Phase equilibria in the pyroxene quadrilateral. J. Petrol. 27, 843–852.

TROMMSDORFF, V. (1990): Metamorphism and tectonics in the Central Alps: the Alpine lithospheric mélange of Cima Lunga and Adula. Mem. Soc. Geol. It. 45, 39–49.

VANCE, D. and O'NIONS, R.K. (1992): Prograde and retrograde thermal histories from the central Swiss Alps. Earth Planet. Sci. Lett. 114, 113–129.

Manuscript received January 20, 1994; accepted May 2, 1994.